

GS305+04-26: Revisiting the ISM around the Cen OB1 stellar association

M. A. Corti^{1,2*}, E. M. Arnal^{1,2*}, R. B. Orellana^{2,3*}

¹ Instituto Argentino de Radioastronomía (CCT-La Plata, CONICET), C.C. No. 5, 1894 Villa Elisa, Argentina

² Facultad de Ciencias Astronómicas y Geofísicas, Universidad Nacional de La Plata, Paseo del Bosque s/n, 1900 La Plata, Argentina

³ Instituto de Astrofísica de La Plata (CCT-La Plata, CONICET), Argentina

Received February 20, 2022; accepted ...

ABSTRACT

Context. Massive stars deeply modify their surrounding ISM via their high throughput of ionizing photons and their strong stellar winds. In this way they may create large expanding structures of neutral gas.

Aims. We study a new large H I shell, labelled GS305+04-26, and its relationship with the OB association Cen OB1.

Methods. To carry out this study we have used a multi-wavelength approach. We analyze neutral hydrogen (H I) line data retrieved from the Leiden-Argentina-Bonn (LAB) survey, new spectroscopic optical observations obtained at CASLEO, and make use of proper motion databases available via Internet.

Results. The analysis of the H I data reveals a large expanding structure GS305+04-26 centered at $(l, b) = (305^\circ, +4^\circ)$ in the velocity range from -33 to -17 km s⁻¹. Based on its central velocity, -26 km s⁻¹, and using standard galactic rotation models, a distance of 2.5 ± 0.9 kpc is inferred. This structure, elliptical in shape, has major and minor axis of 440 and 270 pc, respectively. Its expansion velocity, total gaseous mass, and kinetic energy are ~ 8 km s⁻¹, $(2.4 \pm 0.5) \times 10^5 M_\odot$, and $(1.6 \pm 0.4) \times 10^{50}$ erg, respectively. Several stars of the OB-association Cen OB1 are seen projected onto, and within, the boundaries of GS305+04-26. Based on an analysis of proper motions, new members of Cen OB1 are identified. The mechanical energy injected by these stars could have been the origin of this H I structure.

Key words. Galaxy: kinematics and dynamics – Galaxy: structure – Galaxy: open cluster and associations: individual: Centaurus OB1 – ISM: bubbles – ISM: structure – radio lines: ISM

1. Introduction

Neutral hydrogen emission at $\lambda \sim 21$ -cm shows that the interstellar medium (ISM) of spiral galaxies have a complex morphology, because superimposed on their large scale structure a plethora of different features (arcs, bubbles, chimneys, filaments, holes, loops, shells, supershells, worms, etc) are observed. Among them, large neutral hydrogen shells and their major siblings, the so-called H I supershells, are some of the most spectacular phenomena. Though the origin of the large shells can well be explained by the action of either stellar winds or supernova explosions, or most likely, by their combined effects, the origin of the H I supershells is not well understood yet. The later were discovered by Heiles (1979, 1984). Large shells of neutral hydrogen and H I supershells are usually identified, in a given velocity range, as a minimum in the H I emissivity distribution surrounded by regions of higher emissivity. In order to power the H I supershells an unrealistically large number of massive stars, ranging from hundreds to thousands, would be required. For these extreme cases, alternative processes like gamma-ray bursts (Perna & Raymond 2000) or the infall of high velocity clouds (Tenorio-Tagle 1981) have been invoked. Nevertheless, there is a handful of the catalogued H I supershells for which a particular OB-association has been identified as its likely powering source. Among these, McClure-Griffiths et al. (2001) sug-

gest that the H I supershell GSH305+01-24 was “formed from stellar winds in the Centaurus OB1 association”. Among the arguments in favour of such interpretation the authors quoted that “the morphology of the shell seems to trace the stellar distribution, suggesting an association”. Furthermore, whilst addressing the issue of whether or not GSH305+01-24 could be explained as a wind-driven bubble created by the early type stars of Cen OB1, the Wolf-Rayet star WR 48 (θ Mus) was considered to be a member of the association.

As part of a long term program aimed at improving the optical data (e.g. radial velocity, binarity, spectral types, membership, etc.) of stars considered to be members of OB-associations located in the Southern Hemisphere, new spectroscopic observations were carried out towards most of the early type stars listed by Humphreys (1978) as members of Cen OB1. Furthermore, using Tycho-2 catalogue and applying a new method of proper motion analysis recently developed by Orellana et al. (2010), a substantial revision of the stars thought to be members of Cen OB1 is made.

In the light of the above results it was found that the census of early type stars, those that matter from the wind injection energy viewpoint, is altered to such an extent that makes worth the effort of reviewing the suggested association between Cen OB1 and GSH305+01-24 claimed by McClure-Griffiths et al. (2001).

2. Observational Data

This research was carried out using both new observational data and databases publicly available, namely:

Send offprint requests to: Mariela A. Corti, e-mail: mariela@fcaglp.unlp.edu.ar

* Member of Carrera del Investigador Científico, CONICET-CCT La Plata, Argentina

- a) Spectroscopic observations of sixteen (16) stars listed by Humphreys (1978) as members of Cen OB1 were obtained at Complejo Astronómico El Leoncito (CASLEO)¹ during April 2009. The spectra were obtained using a REOSC Cassegrain echelle spectrographs attached to the 2.15-m "Jorge Sahade" telescope. The detector was a TEK CCD (1024 x 1024 pixels) having pixel size of 24 μ m. A grating of 400 l/mm was used as cross disperser, and the slit width was set either to 250 μ m or 300 μ m. The reciprocal dispersion was 6.6 Å/mm. These spectra covered the wavelength range from 3800Å to 6500Å, and the signal-to-noise ratio is $20 \leq S/N \leq 50$. A He-Ar comparison lamp images were obtained at the same telescope position as the stellar images immediately after or before the stellar exposures. Bias frames were also obtained every night, as well as spectra of the stars HR 2806 and HR 7773 as radial velocity standards. The spectra of several spectral type standards were also obtained along the observing run. All spectra were processed and analysed using the IRAF² package.
- b) Neutral hydrogen line data retrieved from the Leiden-Argentina-Bonn (LAB) survey (Kalberla et al. 2005).
- c) WR 48 proper motion measurements retrieved from the *Centre de Données Astronomiques de Strasbourg* (CDS)³.

3. Results

3.1. Optical spectroscopic

Most of the Cen OB1 stars listed by Humphreys (1978) having spectral types earlier than A2 were observed using the CASLEO telescope. They are listed in Table 1. Using these data and the spectral type catalogue of Walborn & Fitzpatrick (1990) a new spectral classification was derived for each star (see column 4th in Table 1). The star identification is given in the first column, whilst its galactic coordinates (longitude and latitude) are given in the second and third columns, respectively. Using this new spectral types, the intrinsic (B-V)₀ colour index and the absolute visual magnitude M_v matching the spectral type were obtained from Schmidt-Kaler (Th. 1982). With these parameters and adopting a visual extinction $A_v = 3.1 E(B-V)$, where $E(B-V)$ is the stellar colour excess, the stellar distance (seventh column in Table 1) of each star is derived. The photometric magnitudes V and B were corrected from the Tycho-2⁴ system to the Johnson system. The quoted error in the distances stems from an assumed M_v uncertainty of 0.5 magnitudes (Walborn 1972).

Using the IRAF standard reduction package, the stellar heliocentric radial velocity was derived from a gaussian fit to the He I and He II lines present in the stellar spectrum. Later on this heliocentric radial velocity was corrected to the Local Standard of Rest (LSR) (see sixth column Table 2). Since all program stars but two (HD 113432 and HD 114213) were observed twice, those stars having highly discordant individual radial velocity estimates, were identified as possible multiple (SB2 or triple) systems. Based on the radial velocity obtained for those stars assumed to be single, the mean radial velocity of Cen OB1 is -

$24 \pm 14 \text{ km s}^{-1}$. Throughout this paper, all radial velocities are referred to the Local Standard of Rest (LSR).

3.2. Proper motion analysis

3.2.1. WR 48

Large scale catalogues (Hipparcos 1997; Tycho2 2000; PPMX 2008; ASCC2.5 2009) quote quite different, and a first glance even contradictories, proper motions for the Wolf-Rayet WR 48 (\equiv HD113904 \equiv ΘMus). All proper motions in this paper will be expressed in units of milliarcseconds per year (mas/yr). From a thorough analysis of the proper motions provided for this star by the different catalogues, those given by the ASCC2.5 catalogue ($\mu_\alpha \cos \delta, \mu_\delta$) = $(-4.42 \pm 0.79, 2.53 \pm 0.95)$ (Kharchenko 2001) are found to be the most reliable ones and will be adopted in this paper. This conclusion is based on the following considerations:

- a) It is a well known fact that due to the short time interval covered by the Hipparcos mission (less than four years), quite often the proper motions provided by this catalogue are not as good as their formal standard errors seems to indicate. This situation is even worse for double or multiple stars (Urban et al. 2000; Vondrak 2004), because in these cases the quoted proper motions may reflect the *instantaneous* proper motion rather than the *mean* value needed for long term extrapolation. The Hipparcos catalogue quotes the components of the proper motion ($\mu_\alpha \cos \delta, \mu_\delta$) = $(-5.35 \pm 0.59, -2.23 \pm 0.68)$ (Perryman & ESA 1997).
- b) The reliability of the components of the proper motions of WR 48 ($\mu_\alpha \cos \delta, \mu_\delta$) = $(-1.9 \pm 1.3, 19.0 \pm 1.3)$ (Hog et al. 2000) quoted by the Tycho-2 catalogue, could be evaluated in the light of the so-called "goodness of the fit", that is given by a quality flag parameter (see columns 18 and 19 of Tycho-2 catalogue⁵). "This goodness of fit is the ratio of the scatter-based and the model-based error", and may get values ranging from 0 up to 9. A larger value should be taken as a warning on the proper motion quality. For WR 48 the proper motion in declination has a quality flag of 7.5.
- c) Proper motions retrieved from the Position and Proper Motion Extended catalogue (PPMX) (Röser et al. 2008) having a problem with the least square fit used to derive the proper motion of a given star were signaled with a flag "P". Those quoted for WR 48 ($\mu_\alpha \cos \delta, \mu_\delta$) = $(-0.3 \pm 1.7, 16.6 \pm 1.8)$ have such a flag.

3.2.2. Cen OB1

The stellar association Cen OB1 was first reckoned as such based on spectrophotometric study of Humphreys (1978). A total of 29 stars were listed as members of this association (see Table 8 of Humphreys (1978)). The distance modulus derived by Humphreys (1978) for this association is 11.9 magnitude (~ 2.4 kpc). Later on, based on a photometric work of Humphreys & McElroy (1984), the members of Cen OB1 was increased to 106 stars.

Since long time ago stellar proper motions have been used to established the likelihood of membership of a given star to a given stellar grouping such as an open cluster or an OB-association (Dias et al. 2002; de Zeeuw et al. 1999, and references therein). Nowadays, the availability of proper motion catalogues containing thousands of measurements of stars (e.g.

¹ Operated under agreement between CONICET, SeCyT, and the Universities of La Plata, Córdoba and San Juan, Argentina

² IRAF is distributed by NOAO, operated by AURA, Inc. under an agreement with NSF

³ <http://cdsweb.u-strasbg.fr/>

⁴ <http://www.rssd.esa.int/index.php?page=Overview&project=HIPPARCÓS> <http://webviz.u-strasbg.fr/viz-bin/VizieR?-source=I%2F259>

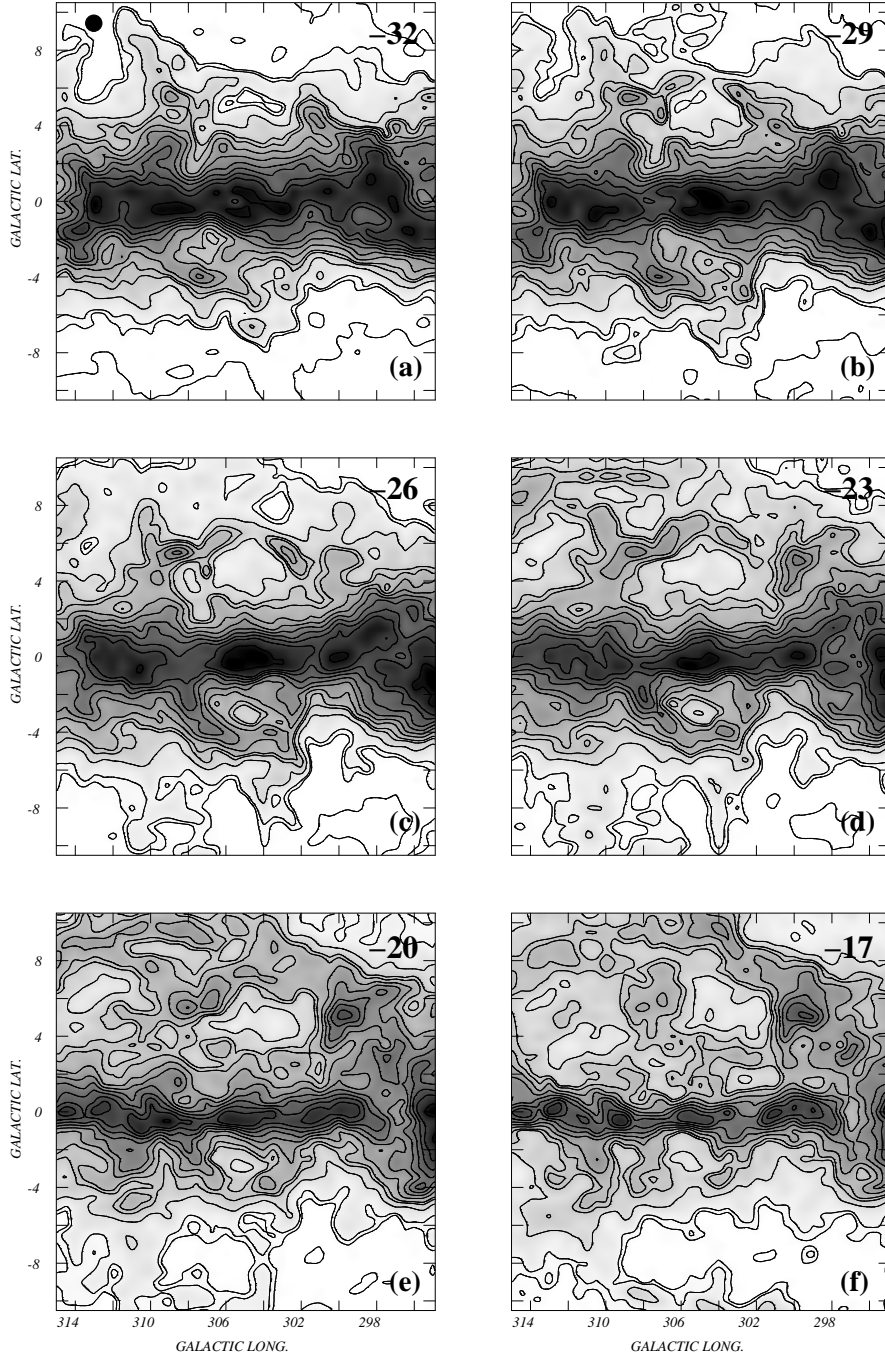


Fig. 1. Mosaic of H I mean brightness temperature in selected velocity ranges within -33 to -16 km s^{-1} . Each image is a mean of three individual images. The central velocity of each image is indicated at the inner top right corner. The filled circle drawn in the upper left corner of the H I image at -32 km s^{-1} indicates the angular resolution of the H I data. The lowest and highest contours are 15 K and 105 K, respectively, while the contour spacing is 5 K until 50 K and 15 K from there onwards. The dark grey areas represent regions with high H I emissivity.

Hipparcos 1997; Tycho2 2000; PPMX 2008; ASCC2.5 2009) distributed all over the sky, offers the chance of routinely using proper motions-based techniques in order to improve our knowledge on the number of stars that may be related to an already known stellar grouping.

Since according to McClure-Griffiths et al. (2001) GS305+01-24 was “formed by the stellar winds in the Centaurus OB1 association”, it is worth making an identification as likely as possible of its members.

To identify the members of Cen OB1 based on the analysis of existing large scale proper motion catalogues, a two steps procedure was followed. Firstly, the technique of Orellana et al. (2010) was applied to the Hipparcos Catalogue (that is complete down to a visual (V) magnitude ranging from 7.3 to 9.0 (depending on spectral type), on a circular area of radius 7° centered at $(l, b) = (305^\circ, +0^\circ)$. The reason for selecting such a large search radius is twofold, namely: *i)* To be able to search for stars candidate to be members of Cen OB1 on an angular area

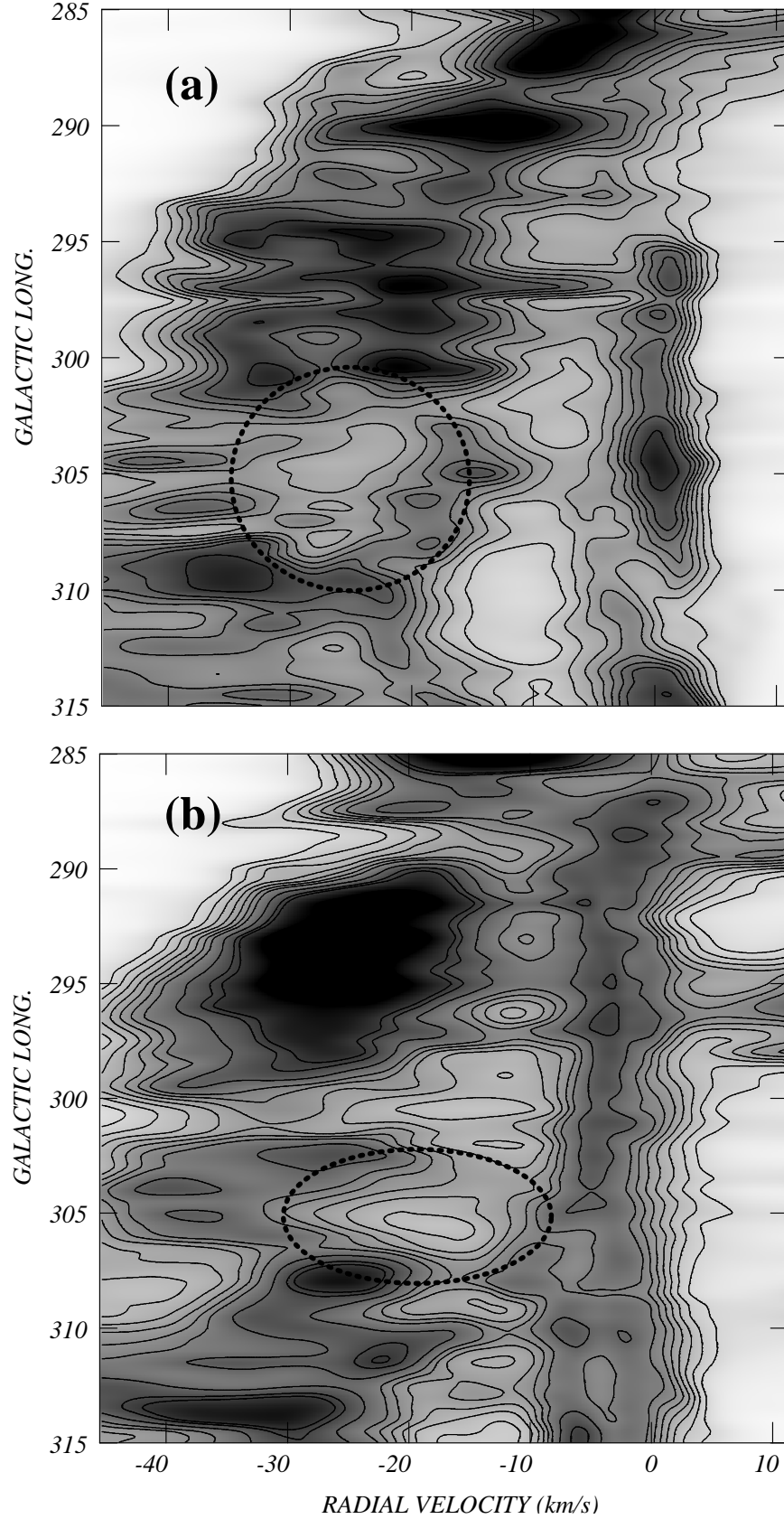


Fig. 2. Velocity-galactic longitudinal diagram of the mean brightness temperature distribution in two different ranges of galactic latitude. The upper panel shows the velocity-galactic longitudinal diagram for $3.5 \leq b \leq 4.0$. The dotted circumference signals the location of Feature A. (see text). The lower panel shows the same diagram for the galactic latitude strip $-3.0 \leq b \leq -2.5$. The dotted ellipse marks the location of Feature B.

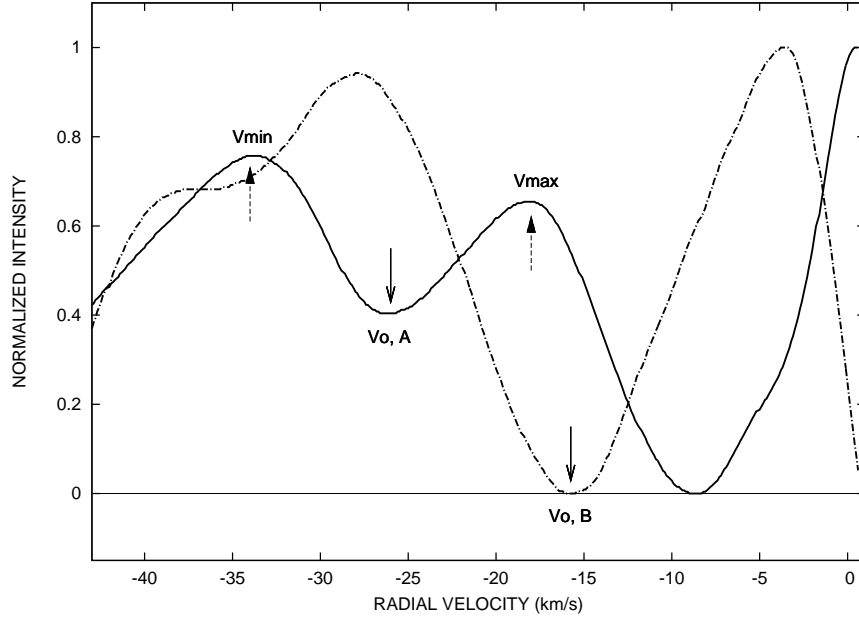


Fig. 3. Normalized mean H I brightness temperature profiles for the range $298^\circ \leq l \leq 312^\circ$ (Feature A, continuous line) and between $300^\circ \leq l \leq 310^\circ$ (Feature B, dash-dotted line profile). The arrows mark the mean radial velocity for Feature A ($V_{o,A}$) and Feature B ($V_{o,B}$), respectively.

larger than the one covered by the stars quoted by Humphreys (1978) as members of the association; *ii*) To include all stars located within a solid angle comparable to, or slightly larger than the region covered by GS305+01-24 (McClure-Griffiths et al. 2001). Having in mind that the short time interval covered by the Hipparcos mission conspires against the accuracy of its quoted proper motions, in a second step the same technique was applied to an square area of 7° in size of the Tycho-2 catalogue. This area is also centered at $(l, b) = (305^\circ, +0^\circ)$. Bearing in mind that the Tycho-2 catalogue is 90% complete down to a visual (V) magnitude $V=11.5$ we should be able to identify all supergiant stars, regardless of their spectral type, that may belong to Cen OB1, and all main sequence and giant stars whose spectral types are earlier than B 3 V and B 6 III, respectively. In this way, 105 stars were identified as possible members of Cen OB1.

Restricting the above sample only to those stars having both a spectral type classification and photometric data, and retaining from this sub-sample only those stars whose distance lie within $\pm 1\sigma$ of the mean distance, a total of 54 stars were identified as likely candidates to be members of Cen OB1. These stars are listed in Table 2. The mean spectrophotometric distance of this grouping turns out to be 2.6 ± 0.4 kpc, in good agreement with previous Cen OB1 distance estimates (Humphreys 1978; Humphreys & McElroy 1984; Kaltcheva & Georgiev 1994). Comparing the list of 106 stars of Humphreys & McElroy (1984) with our listing of 54 stars (see Table 2), it is found that only $\sim 24\%$ of the stars are common to both sets. In the same sense, only 10 out of the 22 stars originally listed by Humphreys (1978) as members of Cen OB1 are present in our sample.

To be considered as a candidate star to be member of Cen OB1, a given star must have a membership probability (P_a) higher than or equal to 0.5 according to the Bayesian criterion. This means that if Φ_a represents the spatial function distribution of all stars in the region belonging to the association and Φ_f rep-

resents the spatial distribution of all non-member stars present in the same region (see Sect. 4.1 of Orellana et al. (2010)), then

$$P_a = \frac{\Phi_a}{\Phi_f + \Phi_a} \quad (1)$$

The components of the mean proper motion of Cen OB1 stars are $(\mu_\alpha \cos \delta, \mu_\delta) = (-4.65 \pm 0.15, -0.92 \pm 0.12)$.

A comparison of this proper motion with the one adopted for WR 48, indicates that whilst the later is moving from lower galactic latitudes towards the galactic plane, the association Cen OB1, as a whole, is moving in the other way. Therefore, WR 48 is unlikely to belong to this association.

3.3. One single large H I structure ?

Relying on the central radial velocity ($V_o = -24 \text{ km s}^{-1}$) and the expansion velocity ($V_{exp} \sim 7 \text{ km s}^{-1}$) of GS305+01-24 derived by McClure-Griffiths et al. (2001), the H I brightness temperature distribution covering the velocity range from -40 to -10 km s^{-1} was re-analysed within the region delimited by $290^\circ \leq l \leq 320^\circ$ and $-10^\circ \leq b \leq +10^\circ$ using the LAB H I survey Kalberla et al. (2005). Though this survey has a lower angular resolution (HPBW= $34'$) than other available databases (e.g. Kalberla et al. (2005), HPBW= $14'.4$), the difference in angular resolution plays only a minor role when the object under study, like the one we are dealing with, has angular dimensions of several degrees. The main observational characteristics of this distribution are shown in Fig.1, where a mosaic of six H I images spanning the velocity from -32 to -17 km s^{-1} is shown.

Before describing the H I images, a word of caution is in place. Considering that towards the inner part of the Galaxy the radial velocity-to-distance transformation is double-valued, the straightforward interpretation that the H I minima observed, for example, in Fig. 1(c) represent *different* structures may not be correct, because in a given radial velocity range, H I emission arises from two different locations along the line of sight.

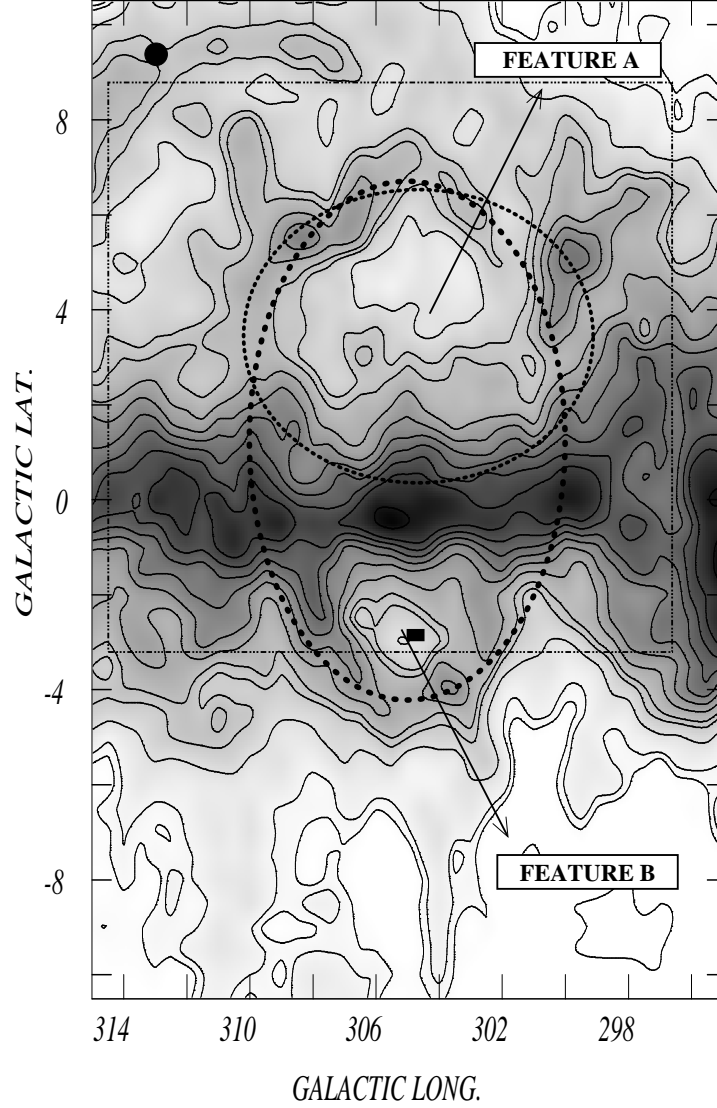


Fig. 4. Grey-scale representation of the mean H I brightness temperature in the velocity range -26 to -19 km s^{-1} . The light dot ellipse represents the least square fit to the H I peaks defining GS305+04-26. The location of GSH305+01-24 (McClure-Griffiths et al. 2001) is depicted by a dark dot ellipse. The dash-dotted rectangle delimits the region shown in Fig. 5. The small black rectangle shows the position of the star WR 48. The angular resolution of these data is given by the filled dot drawn in the upper left corner.

Therefore, a large single H I minima extending both above and below the galactic plane will *always* appear bisected at lower galactic latitudes by a strong band of galactic H I emission, giving the impression of two different minima when in reality is a single structure. Having clarified this point, we shall proceed to briefly describe, only from a morphological point of view, the main characteristics of the H I emission observed along the velocity range -32 to -17 km s^{-1} . The images at -26 km s^{-1} (Fig. 1(c)), -23 km s^{-1} (Fig. 1(d)), and -20 km s^{-1} (Fig. 1(e)) the H I distribution shows the presence of two well developed H I minima in the brightness temperature distribution. The one located at positive galactic latitudes (labelled Feature A from here onwards) roughly centred at $(l, b) = (305^\circ, +4^\circ)$ is ovoidal in shape ($\Delta l, \Delta b \sim (10^\circ, 6^\circ)$) and has its major axis almost parallel to the galactic plane. The minimum located below the galactic plane (Feature B from here onwards), also elliptical in shape, is centred at $(l, b) = (305^\circ, -3^\circ)$ and has its major axis along a position angle of $\sim 60^\circ$. Position angles are measured counterclockwise from north galactic pole direction. At more negative radial velocities

than those mentioned above (see Fig. 1) Feature A remains visible till $-32/-30$ km s^{-1} , where it begins to become undetectable against the overall galactic H I emission at those velocities. On the other hand, Feature B is hardly seen at -32 km s^{-1} (Fig. 1(a)). The noticeable H I minimum seen at $(l, b) = (307^\circ, -2.5^\circ)$ should not be mistaken with Feature B, because the former, first detected at $-29/-28$ km s^{-1} , is located closer to the galactic plane and towards increasing galactic longitudes than Feature B. At radial velocities more positive than -23 km s^{-1} , though both H I minima are easily identifiable in the H I distribution at -20 km s^{-1} , Feature A begins to lose identity at -17 km s^{-1} , whilst at the same velocity Feature B remains clearly visible. Therefore, from Fig. 1 it appears that Feature A and Feature B may not be detectable along the *same* velocity interval. In order to further analyse this point, radial velocity versus galactic longitude images, at specific intervals of galactic latitude, were constructed. In Fig. 2 two such images are shown. The upper panel depicts the mean H I emission distribution at $3.5 \leq b \leq 4.0$, whilst the lower one corresponds to the galactic latitude interval $-3.0 \leq b \leq -2.5$. In both panels

the local H I emission is depicted by the almost straight ridge of emission seen at both slightly positive (*upper panel*) and slightly negative velocities (*lower panel*). The minimum of H I emission corresponding to either Feature A or Feature B are encircled in both panels by thick-dashed figures to help the reader to identify them. Admittedly, the above argument is only a qualitative one. In Fig. 3 the normalized mean brightness temperature as a function of radial velocity, as derived from Fig. 2 for different galactic longitude ranges, are shown. In Fig. 3 the continuous line shows the normalized mean brightness temperature for the range $298^\circ \leq l \leq 312^\circ$ of Fig. 2a), whilst the dot-dashed line shows the behaviour observed for Feature B in Fig. 2b). In this case the interval used to construct the normalized H I profile is $300^\circ \leq l \leq 310^\circ$. The normalized emission was computed by subtracting from each point the minimum value of the corresponding scan (19 K and 31 K for Features A and Feature B, respectively) and then dividing by the corresponding maximum (27.2 K and 21.1 K for Features A and B, respectively). Clearly enough, Fig. 3 shows that the mean radial velocity and the FWHM of both features, namely $V_{o,A} = -26 \text{ km s}^{-1}$ and 9 km s^{-1} , respectively, for Feature A, and $V_{o,B} = -16 \text{ km s}^{-1}$ and 14 km s^{-1} , respectively, are different. This is not the expected behaviour in case *both* features *were* part of a single large H I void, because in this case one would expect that the mean radial velocity of both features (A and B) were, within errors, similar and the FWHM of Feature B were smaller than the corresponding to Feature A. Mean radial velocities and FWHM were derived from a Gaussian fitting and both are accurate to within $\pm 1 \text{ km s}^{-1}$.

Using the linear fit and the power law fit of the galactic rotation model of Fich et al. (1989) the kinematic distances of both H I structures turned out to be $2.5 \pm 0.9 \text{ kpc}$ (Feature A) and $1.7 \pm 0.7 \text{ kpc}$ (Feature B), respectively. The quoted distances are a mean weighted value of the individual distances provided by the different models. The weight of the individual distance determinations stems from the assumption of an uncertainty of $\pm 8 \text{ km s}^{-1}$ due to non-circular motions (Burton 1988).

Therefore, under the assumption that both shells have a line-of-sight dimension comparable to those observed in the plane of the sky, and exclusively relying on the derived mean distances for both H I features, the line of sight width of both shells would be insufficient to overlap them in space, even within the large errors quoted for the individual distances of both features.

Based on above, it is believed that Feature A and Feature B are *unrelated* H I structures, and not different manifestations of the same feature (GSH305+01-24) as put forward by McClure-Griffiths et al. (2001). In this context, it is worth mentioning that Feature B was interpreted (Cappa de Nicolau & Niemela 1984) as being an H I feature exclusively associated with the Wolf-Rayet star WR 48 ($\equiv \Theta \text{Mus}$), that is not a member of Cen OB1.

The mean brightness temperature distribution in the range -26 to -19 km s^{-1} is shown in Fig. 4. The shell GSH305+01-24 reported by McClure-Griffiths et al. (2001) is shown as a thick dark dotted ellipse, whilst the approximate boundaries of Feature A is depicted by a light dotted line. Following the standard nomenclature, Feature A from here onwards will be referred to as GS305+04-26. The high latitude border of this structure has a mean brightness temperature of $\sim 20 \text{ K}$ above the surrounding background galactic emission, a fact that favours its clear identification. Unfortunately, the low latitude extreme of GS305+04-26 is not detected because is projected onto the strong ($T_b \sim 90 \text{ K}$) emission arising from the H I located at the far kinematic distance ($\sim 7.5 \text{ kpc}$) along this line of sight, making the effort of attempting to disentangle it from the overall galactic H I emis-

sion a pointless task. The physical parameters of GS305+04-26 are derived from a least square fit of an ellipse to the H I peaks defining the shape of GS305+04-26 above $b = 2^\circ$. From this fit, shown in Fig. 4 by the a thin dotted line, the supershell center is $(l, b) = (305^\circ, +4^\circ)$ and the major and minor angular semi-axis of GS305+04-26 are $\sim 5^\circ$ and 3° , respectively. The fitting errors of the supershell centre are ± 0.3 . At the distance of GS305+04-26 these angular dimensions are equivalent to $220 \pm 70 (R_{\text{max}})$ and $135 \pm 40 (R_{\text{min}})$ pc, respectively.

Under the assumption of an optically thin H I emission, the total H I mass of a structure located at a distance d (kpc) that subtends a solid angle Ω (squared arc min) is given by

$$M_{\text{HI}} = 0.0013 d^2 \Delta V \Delta T_B \Omega (M_\odot) \quad (2)$$

where ΔV is the velocity interval covered by the structure, expressed in km s^{-1} , and ΔT_B (K) is the mean brightness temperature of the structure defined as $\Delta T_B = |T_{\text{sh}} - T_{\text{bg}}|$, where T_{sh} refers to the mean shell H I brightness temperature, and T_{bg} is the brightness temperature defining the outer level of the H I structure. In this way, the neutral hydrogen mass of GS305+04-26 is of the order of $M_{\text{HI}} = (1.8 \pm 0.4) \times 10^5 M_\odot$. Assuming a helium abundance of 34% by mass, the *total* gaseous mass of GS305+04-26 is about $M_t = (2.4 \pm 0.5) \times 10^5 M_\odot$.

The expansion velocity plays a key role (along with the shell's total mass) at the time of evaluating the shell's total kinetic energy. One way of determining this parameter stems from the use of position-position H I images (e.g. those shown in Fig. 1) of the feature under study. In this case the expansion velocity (V_{exp}) is determined making use of the maximum approaching (V_{max}) and maximum receding (V_{min}) radial velocities of those H I features identified as belonging to the expanding structure. Applying this procedure, an expansion velocity - $V_{\text{exp}} = 0.5 \times (V_{\text{max}} - V_{\text{min}})$ of $\sim 6 \text{ km s}^{-1}$ is derived. Generally speaking, V_{exp} determined in this way is a lower limit to the real expansion velocity, because 'extreme'-velocity gas associated with the expanding H I feature could be missed owing to confusion effects with the overall galactic H I emission. Another way of determining V_{exp} is based on the use of velocity-position (either galactic latitude or galactic longitude) diagrams. To evaluate V_{exp} the normalized H I brightness temperature profile shown in Fig. 3 (continuous line) is used. By making a Gaussian fit to the H I emission peaks, V_{max} and V_{min} can be derived along with $V_{o,A}$ that corresponds to the velocity between V_{max} and V_{min} where the minimum value of the H I emission is observed. We derived $V_{o,A} = -26 \pm 1 \text{ km s}^{-1}$. The approaching gas is observed at $V_{\text{min}} = -34 \text{ km s}^{-1}$ and the receding gas is observed at $V_{\text{max}} = -17 \text{ km s}^{-1}$. Therefore, the velocity extent of the observed H I emission associated with GS305+04-26 is consistent with an expansion velocity of $V_{\text{exp}} \approx 8 \pm 1 \text{ km s}^{-1}$. Adopting this value for V_{exp} and using the total mass calculated for GS 305+04-26, the kinetic energy ($E_k = 0.5 M V_{\text{exp}}^2$) of the expanding structure is $E_k \sim (1.7 \pm 0.4) \times 10^{50} \text{ erg}$.

The dynamic (t_{dyn}) age of GS305+04-26 was derived adopting the Weaver et al. (1977) analytic solutions for a thin expanding shell created by a continuous injection of mechanical energy. Under this assumption the dynamic age is given by

$$t_{\text{dyn}} = 0.55 \times 10^6 R_s / V_{\text{exp}} (\text{yr}) \quad (3)$$

where R_s is the radius of the structure, expressed in units of pc. The expansion velocity is given in units of km s^{-1} and the constant in Eq. 3 represents the mean value between

the energy and momentum conserving cases. Adopting for $R_s = \sqrt{(R_{max} \times R_{min})}$, the harmonic mean of the major and minor semi-axes, and using an expansion velocity of 8 km s^{-1} , a $t_{dyn} \sim 10^7 \text{ yr}$ is derived.

4. Discussion

4.1. Origin of GS 305+04-26.

Could GS 305+04-26 have been created by the stellar winds and supernova explosions of the most massive members of Cen OB1? Under the assumption that all stars listed in Table 2 are actually members of Cen OB1, and using a very simple geometrical model, we shall attempt to answer the previous question. In our model we shall also assume that all the stars belonging to Cen OB1 were at the beginning closely packed at the centroid of GS 305+04-26.

The total mechanical energy (E_w) injected by a star along its lifetime is given by $E_w = L_w \tau$, where L_w is the stellar mechanical luminosity ($L_w = 0.5 \dot{M} v_\infty^2$) and τ is the age of the star. Under the assumption of solar metallicity, the stellar mass loss rate (\dot{M}) and the wind terminal velocity (v_∞), were derived from de Jager et al. (1988),

$$\log \dot{M} = 1.769 \log L/L_\odot - 1.676 \log T_{eff} - 8.158 \quad (4)$$

$$\log v_\infty = 1.23 - 0.3 \log L/L_\odot + 0.55 \log M/M_\odot + 0.64 \log T_{eff} \quad (5)$$

where L is the stellar luminosity expressed in solar luminosity units, and T_{eff} is the effective stellar temperature expressed in K.

In Eq. (5), M indicates the mass of the star (in solar mass units). The value of v_∞ agree with observations to within 20%. For a given spectral type, the basic stellar parameters (L , M and T_{eff}) were adopted from the values given by Schmidt-Kaler (Th. 1982).

In order to provide an estimate for the stellar mass, using both the spectral type given in column fourth of Table 2, and the relationship between stellar mass and effective temperature given by Schmidt-Kaler (Th. 1982), a mass estimate (eight column of Table 2) was derived for every star. Following Schaller et al. (1992) the age (τ) is derived. For those stars belonging to the main sequence, an age estimate was drawn under the assumption that they are in the nuclear hydrogen burning phase, whilst for the evolved stars (those having luminosity classes other than V) their ages were determined after adding up together the time spent in the hydrogen, helium and carbon nuclear burning phases. The stellar ages are given in column nine of Table 2. Following the above procedure, late B-type stars with uncertain spectral classification (HD 109253, HD 110912, HD 111121, and HD 116864) have masses, and hence stellar ages, quite uncertain. Consequently, neither M nor τ was derived for these four stars. The total mechanical energy injected by the stars of Cen OB1 is the sum of the contributions of all stars along their lifetime. Based on above, the total mechanical energy input by the stars of Cen OB1 into its local ISM is $(2.7 \pm 0.1) \times 10^{51} \text{ erg}$. Using de Jager et al. (1988) to estimate the wind terminal velocity, and the parameterization of the mass-loss rate of Lamers & Leitherer (1993),

$$\log \dot{M} = 1.738 \log L/L_\odot - 1.352 \log T_{eff} - 9.547 \quad (6)$$

results in a total mechanical energy input lower by almost 30%. Equation (6) is the average relation for \dot{M} in a sample of Galactic O stars studied by Lamers & Leitherer (1993).

According to these authors the standard deviation of individual mass-loss rates is $\sigma = 0.23$.

Though theoretical models predict that 20% of the wind injected energy is converted into mechanical energy of an expanding shell (Weaver et al. 1977), from an observational view point the energy conversion efficiency seems to be as low as 2–5 % (Cappa et al. 2003).

Additional sources of energy input may have been present within the boundaries of GS 305+04-26. It is worth pointing out that supernovae explosions (SN_e) may have taken place among the most massive members of Cen OB1. Though there are no supernova remnants catalogued within the solid angle covered by GS 305+04-26, three pulsars located within the boundaries of this shell indicate that SN_e took place in the past. The pulsars are PSR J1253-5820 ($d = 2.2 \text{ kpc}$, $(l, b) = (303^\circ.2, +4^\circ.5)$), PSR J1334-5839 ($d = 2.4 \text{ kpc}$, $(l, b) = (308^\circ.5, +3^\circ.7)$), and PSR J1254-6150 ($d = 2.24 \text{ kpc}$, $(l, b) = (303^\circ.3, +1^\circ.02)$). The characteristic age of the pulsars (τ_c) are $\sim 2 \times 10^6 \text{ yr}$ (PSR J1253-5820), $\sim 5 \times 10^6 \text{ yr}$ (PSR J1254-6150), and $\sim 8 \times 10^7 \text{ yr}$ (PSR J1334-5839), respectively (Manchester et al. 2005). The distance of PSR J1253-5820 has been taken from Noutsos et al. (2008), whilst the distance of the other two is given by Manchester et al. (2005).

From Table 2 there is evidence of continuous star formation, because the stellar ages τ covered the range from ~ 5 to 24 Myr , with a mean value of $12.6 \pm 5 \text{ Myr}$. Bearing in mind the fact of a continuous stars formation, we shall adopt as the age of the association the age of the oldest stars likely to be members of Cen OB1. Hence, Cen OB1 would be $\sim 2 \times 10^7$ years old. The ages of PSR J1253-5820 and PSR J1254-6150 are consistent with the assumption that they could have been born in SN_e of stars members of Cen OB1. On the other hand, PSR J1334-5839 has an age almost an order of magnitude greater than the age of Cen OB1. Bearing this in mind, the massive progenitor star of this pulsar very likely was not a member of Cen OB1 and played no role in the formation of GS305+04-26.

Under the assumption that the progenitors of both pulsars were members of Cen OB1, they may have contributed to the formation of GS305+04-26 in two ways. First, by injecting mechanical energy along their stellar lifetime, and secondly by their final SN_e . A lower limit to the mechanical energy input by the stellar progenitors of the pulsars prior to their explosion as SN_e , could be derived assuming that each stellar progenitor spent a time as a "stellar" object, equal to the age of the oldest star likely to be member of Cen OB1 (HD 109937) minus the pulsar's age. In this way, the progenitors of each pulsars could have been main sequence stars in the range from 10 to $12 M_\odot$. Using Eqs. 4 and 5, both progenitors stars could have injected an extra mechanical energy of $\sim 2.4 \times 10^{51} \text{ erg}$ during their lives as stars.

The effect of supernovae on wind-driven bubble evolution may be similar to that of stellar winds acting as an input energy source (McCray & Kafatos 1987). These authors show that assuming a standard initial mass function for a stellar association having N_* stars with mass greater than $7 M_\odot$, the mean energy input by SN_e is given by $E_{SN} \sim 2.0 \times 10^{49} N_* E_{51} \tau_{OB} \text{ erg}$, where E_{51} is the supernova explosion expressed in units of 10^{51} erg and τ_{OB} is the association's age given in units of 10^6 yr . Inserting $N_* = 2$ and $\tau_{OB} \approx 24 \text{ Myr}$, we obtain $E_{SN} \sim 10^{51} \text{ erg}$. Certainly, the assumption that only two SN_e (those that originated the pulsars we are observing nowadays) took place among the stars of Cen OB1 must be viewed as a gross simplification because in the past more stars of Cen OB1 could have gone through the SN_e phase without leaving observable evidence that those events did happen. If the end stellar product of those hypothetical explosions were pulsars, they could be there and at the same time remain undetected

due to their highly anisotropic emission. Therefore, by assuming that only two SN_e took place, a lower limit is provided to the total energy input in this way to the ISM local to Cen OB1.

Therefore, adding up the energy injected into the ISM by the stellar winds of the stars of Cen OB1 and the progenitor stars of both pulsars, and the energy injected by both SN_e , a total of $(3.6 \pm 0.1) \times 10^{51}$ erg may have been injected into the ISM by the stars of Cen OB1 along their lives. In this case the kinetic energy of GS305+04-26 would imply an energy conversion efficiency of $\sim 3\%$ in very good agreement with the results of Cappa et al. (2003).

4.2. Explaining the off-centre location of Cen OB1

In the ideal case of a group of massive stars being at rest with respect to its local ISM, it is expected that this group will be located at the center of an hypothetical stellar wind bubble blown by this group of massive stars. In the case the stars were not at rest with respect to its surroundings, the stars will likely occupied an eccentric location with respect to the bubble's centre. A look at Fig. 5, clearly shows that most of the Cen OB1 stars are located towards the low latitude and low longitude sector of GS305+04-26. In order to attempt to explain, in general terms, this location, we shall follow the procedure outlined by van der Sluys & Lamers (2003) (after correcting the sign of the w_\odot term in their equation 19) and Cichowolski et al. (2008).

Using the mean proper motions of Cen OB1 ($(\mu_\alpha \cos \delta, \mu_\delta) = (-4.65 \pm 0.15, -0.92 \pm 0.12)$), a radial velocity of $-26 \pm 1 \text{ km s}^{-1}$ and a distance of $2.5 \pm 0.9 \text{ kpc}$ (radial velocity and distance of GS305+04-26) as the original distance of Cen OB1, the stellar peculiar velocity components are

$$v_{pec,r} = -2.2 \pm 14.8 \text{ km s}^{-1},$$

$$v_{pec,l} = 12.4 \pm 30.8 \text{ km s}^{-1},$$

$$v_{pec,b} = -15.6 \pm 4.1 \text{ km s}^{-1},$$

where $v_{pec,r}$, is the peculiar radial velocity, $v_{pec,l}$ the peculiar velocity along galactic longitude, and $v_{pec,b}$ the peculiar velocity along galactic latitude. The corresponding *spatial* peculiar velocity of the star,

$$v_{pec} = \sqrt{v_{pec,r}^2 + v_{pec,l}^2 + v_{pec,b}^2}, \quad (7)$$

is $v_{pec} = 20.0 \pm 18.0 \text{ km s}^{-1}$.

According to van der Sluys & Lamers (2003) only two angles, labelled i and ϕ , are needed to completely define the spatial orientation with respect to the observer of the structure created by a star moving with respect to its ISM with a high peculiar velocity. The angle i is measured from the line of sight towards the observer ($i = 90^\circ$ corresponds to the plane of the sky), whilst ϕ is measured on the plane of the sky, counterclockwise from the tip of the peculiar velocity vector (see Fig. 4 of van der Sluys & Lamers (2003)). Following van der Sluys & Lamers (2003), the above angles are defined as

$$i = \arcsin\left(\frac{v_{pec,r}}{v_{pec}}\right) \quad (8)$$

$$\phi = \arctan\left(\frac{v_{pec,l}}{v_{pec,b}}\right) + \varepsilon \quad (9)$$

where ε is the angle between the line of constant declination and the line of constant galactic latitude at the position of the star. In our case $\varepsilon \sim 1^\circ$, and the angles are $i = 95^\circ \pm 45^\circ$, and $\phi = 140^\circ \pm 70^\circ$.

At first glance, one may think that all stars of Cen OB1 should be seen projected onto the interior of GS305+04-26. Nonetheless, a look at Fig. 5, taking into account, the uncertainties of the major and minor semi-axes of GS305+04-26 (error bars drawn in the lower left corner), shows that 12 stars are definitively located outside the large H I shell. Bearing this in mind, under the assumption that these peculiar velocities are inherent to the process of their formation, the sequence of events put forward by Sancisi (1974) could explain the external position of the stars of Cen OB1 with respect to the expanding H I shell. Certainly, in the case of Cen OB1 stellar winds and not SN_e , as was the case in Per OB2, is the main triggering mechanism of the expansion of GS305+04-26. Though these stars have all the basic ingredients to create around them their own IB (that should be observable as a minimum in the H I brightness temperature distribution towards these stars), these minima are not observed. The lack of detection may be explained by the following facts: *i*) the stars in question are seen projected onto the galactic plane where the H I brightness temperature is high and varies quite rapidly with position; *ii*) The dual-value radial velocity relationship implies that any H I minimum related to an IB located at the near kinematic distance will very likely be filled in by H I emission arising from the far kinematic distance region. Based on above, IB around individual massive stars will be hard to recognize as such when the stars are seen projected towards the galactic plane and the 21-cm line emission is observed with a radiotelescope like the one used to produce the LAB H I all-sky survey.

Summing up, and within their large uncertainties, the bulk peculiar spatial velocity of the stars of Cen OB1 and the angles i and ϕ are consistent with the present day location of Cen OB1 with respect to the centroid of GS305+04-26. The off-center location of PSR J1253-5820 and PSR J1254-6150 is quite consistent with the peculiar spatial velocities of these objects (Cordes & Chernoff 1998).

To explain the location of the OB-association projected onto the southernmost border of GS305+04-26, a peculiar velocity of $10 \pm 5 \text{ km s}^{-1}$ would be needed along $12.6 \pm 5 \text{ Myr}$ (the age of the association). This velocity is, within its large error, consistent with the bulk peculiar motions derived for the stars of Cen OB1. A three dimensional sketch of the relative location of the stars with respect to GS305+04-26, is given in Fig. 6. There, the supershell is represented by the ellipsoid shown in dotted lines. The large triangle-like symbol depicts the projection of a conical structure whose apex is located at the centre of GS305+04-26, and its bisecting line is oriented along the angles i and ϕ derived above. The base of the cone points towards both lower galactic latitudes and longitudes. The aperture of the cone is mostly given by the uncertainty in determining the angle ϕ .

5. Conclusions

Examining the neutral hydrogen distribution towards the area covered by Cen OB1, in the light of new data that redefine the stellar membership of this association, a new large H I shell has been found. This structure, designated GS305+04-26, is elliptical in shape with major and minor axis of 440 and 270 pc, respectively. The velocity interval where GS305+04-26 is observable spans the range from ~ -33 to $\sim -17 \text{ km s}^{-1}$. The central velocity is $-26 \pm 1 \text{ km s}^{-1}$ and its expansion velocity is about $\sim 8 \text{ km s}^{-1}$. The kinematic distance of this large structures is $2.5 \pm 0.9 \text{ kpc}$, and has a total gaseous mass of about $M_t = (2.4 \pm 0.5) \times 10^5 M_\odot$.

Evidence has been provided in the sense that the stellar winds of the 54 stars likely to be members of Cen OB1, may well

explained the kinetic energy of this large structure. The pulsars PSR J1253-5820 and PSR J1254-6150 have both distances and characteristic ages compatible with the idea that they were born as the results of SN_e undergone in the past by massive members of Cen OB1.

The present day eccentric location of the stars of Cen OB1 with respect to the centroid of GS305+04-26 can be understood by the peculiar velocities of the stars with respect to its local ISM.

Comparing the proper motion of the Wolf-Rayet star WR 48 with the bulk proper motions of Cen OB1, it is highly unlikely that the Wolf-Rayet star can be considered a member of the stellar association.

Acknowledgements. This work was partially supported by Consejo Nacional de Investigaciones Científicas y Técnicas CONICET under projects PIP 01299 and 01359, and by Universidad Nacional de La Plata (UNLP) under projects 11/G091 and 11/G096. One of us (M.A. Corti) would like to thank both Dra E. Gualarte Scarone for her help in preparing Fig. 6 and Dr. N. Walborn for providing us with updated information of some of the stellar data quoted in Table 2. We would like to thank the referee for her/his constructive remarks.

References

- Burton, W. B. 1988, The structure of our Galaxy derived from observations of neutral hydrogen (Galactic and Extragalactic Radio Astronomy), 295–358
- Cappa, C. E., Arnal, E. M., Cichowolski, S., Goss, W. M., & Pineault, S. 2003, in IAU Symposium, Vol. 212, A Massive Star Odyssey: From Main Sequence to Supernova, ed. K. van der Hucht, A. Herrero, & C. Esteban, 596–+
- Cappa de Nicolau, C. & Niemela, V. S. 1984, *AJ*, 89, 1398
- Cichowolski, S., Pineault, S., Arnal, E. M., & Cappa, C. E. 2008, *A&A*, 478, 443
- Cordes, J. M. & Chernoff, D. F. 1998, *ApJ*, 505, 315
- de Jager, C., Nieuwenhuijzen, H., & van der Hucht, K. A. 1988, *A&AS*, 72, 259
- de Zeeuw, P. T., Hoogerwerf, R., de Bruijne, J. H. J., Brown, A. G. A., & Blaauw, A. 1999, *AJ*, 117, 354
- Dias, W. S., Alessi, B. S., Moitinho, A., & Lépine, J. R. D. 2002, *A&A*, 389, 871
- Fich, M., Blitz, L., & Stark, A. A. 1989, *ApJ*, 342, 272
- Heiles, C. 1979, *ApJ*, 229, 533
- Heiles, C. 1984, *ApJS*, 55, 585
- Hog, E., Fabricius, C., Makarov, V. V., et al. 2000, *VizieR Online Data Catalog*, 1259, 0
- Humphreys, R. M. 1978, *ApJS*, 38, 309
- Humphreys, R. M. & McElroy, D. B. 1984, *VizieR*
- Kalberla, P. M. W., Burton, W. B., Hartmann, D., et al. 2005, *A&A*, 440, 775
- Kaltcheva, N. T. & Georgiev, L. N. 1994, *MNRAS*, 269, 289
- Kharchenko, N. V. 2001, *Kinematika i Fizika Nebesnykh Tel*, 17, 409
- Lamers, H. J. G. L. M. & Leitherer, C. 1993, *ApJ*, 412, 771
- Manchester, R. N., Hobbs, G. B., Teoh, A., & Hobbs, M. 2005, *AJ*, 129, 1993
- McClure-Griffiths, N. M., Dickey, J. M., Gaensler, B. M., & Green, A. J. 2001, *ApJ*, 562, 424
- McCray, R. & Kafatos, M. 1987, *ApJ*, 317, 190
- Noutsos, A., Johnston, S., Kramer, M., & Karastergiou, A. 2008, *MNRAS*, 386, 1881
- Orellana, R. B., de Biasi, M. S., Bustos Fierro, I. H., & Calderón, J. H. 2010, *A&A*, 521, A39+
- Perna, R. & Raymond, J. 2000, *ApJ*, 539, 706
- Perryman, M. A. C. & ESA, eds. 1997, *ESA Special Publication*, Vol. 1200, The HIPPARCOS and TYCHO catalogues. Astrometric and photometric star catalogues derived from the ESA HIPPARCOS Space Astrometry Mission
- Röser, S., Schilbach, E., Schwan, H., et al. 2008, *A&A*, 488, 401
- Sancisi, R. 1974, in IAU Symposium, Vol. 60, Galactic Radio Astronomy, ed. F. J. Kerr & S. C. Simonson, 115
- Schaller, G., Schaerer, D., Meynet, G., & Maeder, A. 1992, *A&AS*, 96, 269
- Schmidt-Kaler, Th. 1982, In Landolt-Bornstein New Series, Group VI, Vol. 2b. (eds. K. Schaifers & H. H. Voigt), (Springer-Verlag, Berlin)
- Tenorio-Tagle, G. 1981, *A&A*, 94, 338
- Urban, S. E., Wycoff, G. L., & Makarov, V. V. 2000, *AJ*, 120, 501
- van der Sluis, M. V. & Lamers, H. J. G. L. M. 2003, *A&A*, 398, 181
- Vondrak, J. 2004, *Serbian Astronomical Journal*, 168, 1
- Walborn, N. & Fitzpatrick, E. 1990, *PASP*, 102, 379
- Walborn, N. R. 1972, *AJ*, 77, 312
- Weaver, R., McCray, R., Castor, J., Shapiro, P., & Moore, R. 1977, *ApJ*, 218, 377

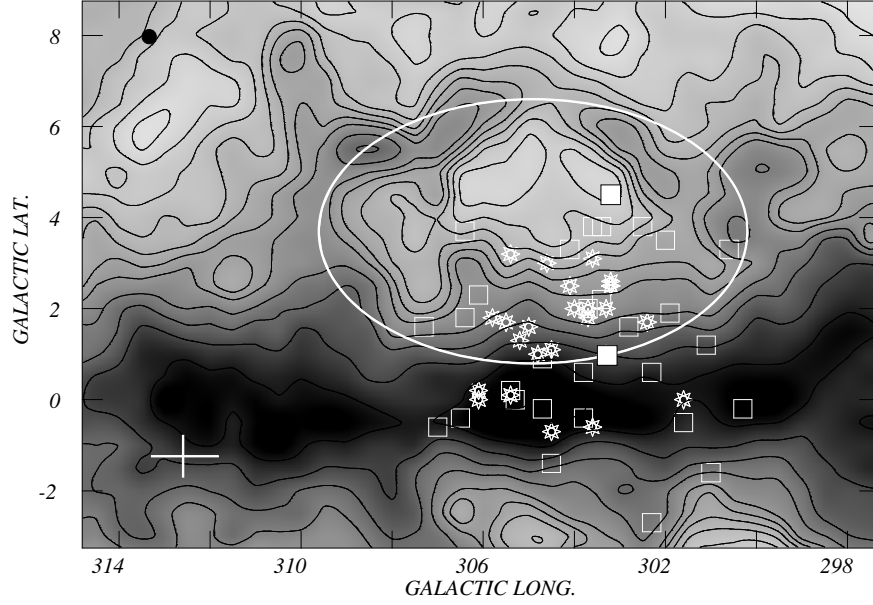


Fig. 5. Blow up of the region delimited by a dash-dot rectangle in the Fig. 4. The angular resolution of these data is given by the filled dot drawn in the upper left corner of the image. The white thin line ellipse represents to GS305+04-26. The white boxes mark the location of the pulsars. The star symbol indicate the location of Cen OB1 members identified as such by both Humphreys & McElroy (1984) and Corti & Orellana (in preparation), whilst the unfilled white squares signal the position of those stars considered to be members of Cen OB1 only by Corti & Orellana (in preparation).

Table 1. New spectral types and radial velocity measurements of Cen OB1 members (according to Humphreys (1978)).

ID	l (°)	b (°)	SpT	V (mag.)	V_{LSR} (km s ⁻¹)	d (kpc)	Commentaries
HD 110639	302.1	+1.5	B1 II-III	8.5	-52 ± 03	1.8 ± 0.5	NGC 4755 NGC 4755 NGC 4755 NGC 4755 SB2
HD 111613	303.0	+2.5	B9-A0 Iab	5.7	-27 ± 03	1.5 ± 0.4	
HD 111904	303.2	+2.5	B9 Ia	5.7	-25 ± 03	2.6 ± 0.6	
HD 111934	303.2	+2.5	B2 Ib	7.0	-31 ± 02	2.0 ± 0.5	
HD 111973	303.2	+2.5	B5 Ia	5.9	-18 ± 04	2.7 ± 0.6	
HD 111990	303.2	+2.5	B3 Ib	6.8	-7 ± 03	1.8 ± 0.5	
HD 112364	303.6	+3.1	B0.5 Ib-a	7.4	-68 ± 12	2.8 ± 0.6	
HD 112842	304.1	+2.5	B3 Ib	7.0	-33 ± 03	2.1 ± 0.5	
HD 113012	304.3	+2.7	B0 Ia	8.1	-22 ± 05	6.9 ± 1.6	
HD 113422	304.5	+1.1	B1 Ia	8.2	-57 ± 04	3.2 ± 0.7	
HD 113432	304.4	-0.7	B1 Ib	8.9	-21 ± 11	2.7 ± 0.6	
HD 113708	304.6	-2.4	B0.2 III	8.1	-16 ± 07	3.1 ± 0.8	
HD 114213	305.2	+1.3	B1 Ia-b	8.9	-2 ± 06	2.2 ± 0.5	
HD 114886	305.6	-0.9	O9 II-III	6.9	-25 ± 08	2.6 ± 0.6	
HD 115363	305.9	-1.0	B1 Ia	7.8	-66 ± 08	3.3 ± 0.9	
HD 116119	306.7	+0.6	B8 Ia	7.9	-34 ± 03	4.3 ± 1.1	SB2

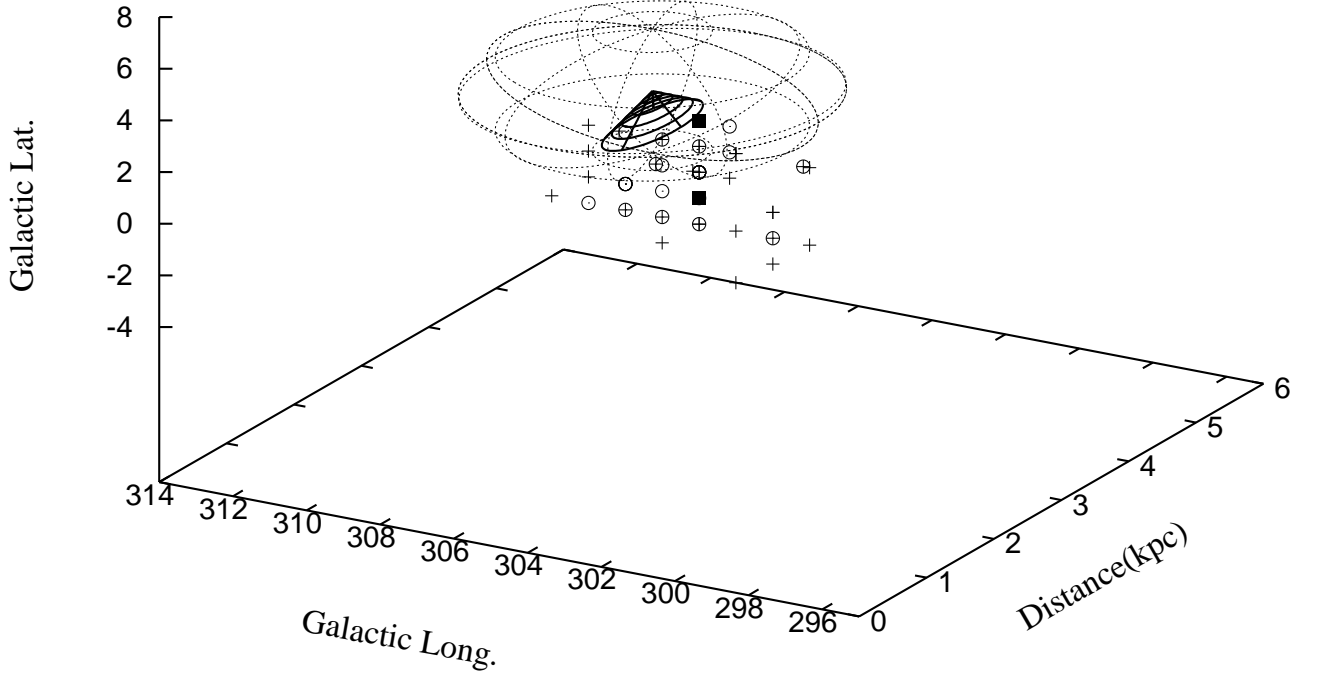


Fig. 6. Three dimensional sketch of GS305+04-26 and the stars members of Cen OB1. The large H I shell is shown as a dotted ellipsoid. The location of both pulsars is given by fill-in black squares. The open circles indicate the location of Cen OB1 members identified as such by both Humphreys & McElroy (1984) and Corti & Orellana (in preparation) whilst the plus sign mark the position of those stars considered to be members of Cen OB1 only by Corti & Orellana (in preparation). The projection of the conical structure referred to in the text is also depicted in this Figure.

⁽¹⁾ (Corti & Orellana, in preparation)

⁽²⁾ Humphreys (1978)

⁽³⁾ Obtained of the SIMBAD Astronomical Database (CDS).

Table 2. Information about the possible members of Centaurus OB1

ID	lg (\odot)	bg (\odot)	SpT	V (mag.)	RV(LSR) (km s $^{-1}$)	d (kpc)	M (M_{\odot})	t (10 6 yrs)	Comments
HD 108516	300.3	-0.2	B2 III	9.5		2.8 ± 0.6	12.0	19.0	
HD 109150	300.6	3.3	B2 II-III	8.6		3.0 ± 0.7	14.5	14.0	
HD 109253	301.0	-1.6	B8 II-III c	9.6		2.3 ± 0.5	–	–	
HD 109505	301.1	1.2	B2 II c	8.0		2.1 ± 0.5	17.0	11.0	
HD 109937	301.6	-0.5	B2-3 III	9.4		2.0 ± 0.5	10.5	24.0	
HD 109978	301.6	0.0	O9 IV	8.9	$-13 \pm 5^{(3)}$	2.7 ± 0.6	22.0	8.1	
HD 110449	301.9	1.9	B2 III c	9.3		2.6 ± 0.6	12.0	19.0	
HD 110597	302.0	3.5	B8 II	9.5		2.3 ± 0.5	11.4	21.0	
CD-64 654	302.3	-2.7	B1 V	9.7		2.2 ± 0.5	13.4	16.0	
HD 110912	302.3	2.1	B8 II-III	9.8		2.2 ± 0.5	–	–	
HD 110984	302.4	1.7	B1 II-III	9.0		2.1 ± 0.5	20.0	9.2	
HD 111121	302.5	3.8	B8-9 II-III	9.6		2.7 ± 0.6	–	–	
HD 111579	302.8	1.6	B2 Ib-II	9.1		2.1 ± 0.5	19.5	9.5	
CP-59 4552	303.2	2.5	B1 III	8.2	$-21^{(3)}$	2.0 ± 0.5	15.4	13.0	NGC 4755 $^{(2)}$
HD 111904	303.2	2.5	B9 Ia $^{(1)}$	5.8	$-25 \pm 3^{(1)}$	2.6 ± 0.6	16.6	12.0	NGC 4755 $^{(2)}$
HD 111934	303.2	2.5	B2 Ib $^{(1)}$	6.9	$-31 \pm 2^{(1)}$	2.0 ± 0.5	22.0	8.1	NGC 4755 $^{(2)}$
HD 111973	303.2	2.5	B5 Ia $^{(1)}$	5.9	$-18 \pm 4^{(1)}$	2.7 ± 0.6	20.0	9.2	NGC 4755 $^{(2)}$
HD 112026	303.3	2.0	B0.5 IV	8.7		2.7 ± 0.6	16.3	12.0	
HD 112147	303.4	3.8	B0 IV pe	9.1		3.0 ± 0.7	18.7	10.0	
HD 112181	303.4	2.2	B2-3 II-III	8.8		2.0 ± 0.5	13.4	16.0	
HD 112364	303.6	3.1	B0.5 Ib-a $^{(1)}$	7.4	$-68 \pm 12^{(1)}$	2.8 ± 0.6	25.0	7.0	SB2
HD 112366	303.6	-0.6	B6 Iab-b	7.6	$-7 \pm 2^{(3)}$	2.1 ± 0.5	19.0	9.8	
HD 112382	303.6	3.8	B4 II	9.0		2.6 ± 0.6	15.0	14.0	
HD 112471	303.7	2.0	B1 II-III	8.8		2.4 ± 0.6	20.0	9.2	
HD 112485	303.7	2.0	B2 III	9.5	$-15^{(3)}$	3.0 ± 0.7	12.0	19.0	
HD 112497	303.7	1.8	B1-2 II-III	8.4		2.2 ± 0.5	15.9	12.0	
HD 112637	303.8	-0.4	B2 III c	9.6		2.2 ± 0.5	12.0	19.0	
HD 112661	303.8	0.6	B0.5 III-IV	9.3		2.0 ± 0.5	17.0	11.3.0	
HD 112784	304.0	2.3	O9.5 III	8.3	$-34 \pm 5^{(3)}$	3.2 ± 0.7	21.7	8.3	
HD 112842	304.1	2.5	B3 Ib $^{(1)}$	7.1	$-33 \pm 3^{(1)}$	2.1 ± 0.5	21.1	8.6	
HD 112852	304.1	3.3	B8-9 II	9.9		2.6 ± 0.6	11.0	22.0	
HD 113421	304.6	3	B0 Vn	9.4	$-33^{(3)}$	2.6 ± 0.6	17.5	11.0	
HD 113422	304.5	1.1	B1 Ia $^{(1)}$	8.3	$-57 \pm 4^{(1)}$	3.2 ± 0.7	23.0	7.7	
HD 113432	304.4	-0.7	B1 Ib $^{(1)}$	8.9	$-21 \pm 11^{(1)}$	2.7 ± 0.6	23.0	7.7	
HD 113606	304.5	-1.4	O7	8.7		2.3 ± 0.5	31.4	5.6	
HD 113742	304.7	0.9	B1-2 III	9.2		2.4 ± 0.5	13.7	16.0	
HD 113754	304.7	-0.2	O6-7	9.5	$-25 \pm 2^{(3)}$	2.8 ± 0.6	34.2	5.2	
CP-61 3452	304.8	1.0	O9.5 II c	9.3		2.8 ± 0.6	22.0	8.1	
HD 114011	305.0	1.6	B4 Ib-II	9.3	$-34 \pm 5^{(3)}$	3.1 ± 0.7	17.7	11.0	
HD 114213	305.2	1.3	B1 Ia-b $^{(1)}$	8.9	$-2 \pm 6^{(1)}$	2.2 ± 0.5	23.0	7.7	
HD 114394	305.4	3.2	B0.5 IV (N)	8.2		2.1 ± 0.5	16.3	12.0	
HD 114478	305.3	0.0	B1 Ib-II	8.7	$-1^{(3)}$	2.8 ± 0.6	21.1	8.6	
HD 114669	305.4	0.2	B5 II	9.1		2.7 ± 0.6	14.5	14.0	
HD 114737	305.4	0.1	O9 III	8.0		2.8 ± 0.6	23.4	7.6	
CP-60 4528	305.5	1.7	B1 III	8.8	$-25^{(3)}$	2.2 ± 0.5	15.4	13.0	
CP-60 4551	305.8	1.8	B1 III (N)e	9.8		2.3 ± 0.5	15.4	13.0	
HD 115223	306.4	3.7	A0 Ib-II	8.7		3.0 ± 0.7	13.0	17.0	
HD 115455	306.1	0	O7.5 III	8.0	$-44 \pm 14^{(3)}$	3.1 ± 0.7	29.0	6.0	
HD 115497	306.4	3.7	B8-9 II	9.7		2.8 ± 0.6	11.0	22.0	
CP-61 3576	306.1	0.2	B0.5 V	9.5	$-40 \pm 69^{(3)}$	2.2 ± 0.5	14.9	13.7	
HD 115666	306.4	1.8	B7 IIc	9.4		2.8 ± 0.6	12.5	18.0	
HD 116121	306.5	-0.4	O9.5 V	9.3		3.4 ± 0.8	19.0	9.8	
HD 116403	307.3	1.6	B5 II-III	9.0		3.1 ± 0.7	10.7	23.0	
HD 116864	307.0	-0.6	B9 II-III	9.1		2.4 ± 0.5	–	–	